Breaking with Light: Stimuli-Responsive Mesoporous Organosilica Particles

Pierre Picchetti,[†] Brian N. DiMarco,[†] Leana Travaglini,[*,†] Yang Zhang,[†] M. Carmen Ortega-Liebana,[†] and Luisa De Cola[*,†,‡]

[†]CNRS, ISIS UMR 7006, Université de Strasbourg, 8 allée Gaspard Monge, 67000 Strasbourg, France
[‡]Institut für Nanotechnologie (INT) - Building 640, Karlsruhe Institute of Technology (KIT) - Campus Nord, Hermann-von-Helmholtz-Platz 1, 76344 Eggenstein-Leopoldshafen, Germany

Ⓢ *Supporting Information*

ABSTRACT: Stimuli-responsive particles have gained considerable interest in many fields of materials science. Among the various possible triggers, light is particularly advantageous due to its easy and efficient spatiotemporal control. In this work, we report the synthesis of a novel light-cleavable bis-alkoxysilane linker and its use for the preparation of mesoporous organosilica particles. We demonstrate that the resulting porous particles can be completely degraded upon exposure to UV light. These light-breakable nanocontainers can encapsulate a large variety of molecules, and they are able to quantitatively release their cargo upon light exposure. We proved the loading and release of a biologically important molecule, provitamin D3, upon UV-light irradiation.
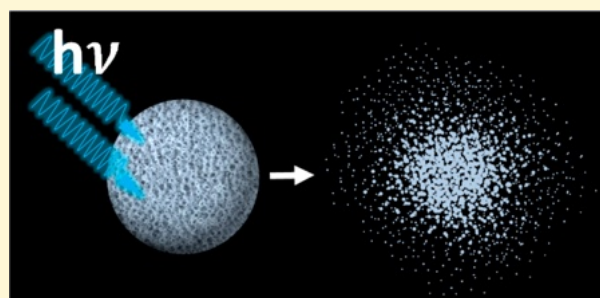
1. INTRODUCTION

Mesoporous organosilica particles have been widely explored as catalysis supports,[1−5] as adsorbents[6−9] and in sensing applications.[10,11] More recently, they have attracted considerable interest for their use in biomedical-related applications.[12−16] Mesoporous organosilica particles are typically prepared by acid- or base-catalyzed hydrolysis and polycondensation of bis-silanes of the type $(RO)_3-Si-R-Si-(OR)_3$ (R = organic moiety), with or without a silica precursor, usually an alkoxysilane such as tetraethyl orthosilicate (TEOS), in the presence of a surfactant that functions as the structure-directing agent. Contrary to conventional postgrafting techniques, by using this method it is possible to embed organic moieties in the silica framework and endow the material with additional and specific functionalities, thereby tuning the particle physicochemical properties. In particular, this approach has been proven successful in designing mesoporous organosilica particles with enhanced degradation.[17,18] For example, breakable particles have been successfully obtained by introducing redox-cleavable disulfide[19−21] and diselenide bonds,[22] enzymatically degradable amide bonds,[23,24] and functional groups that can be hydrolyzed, such as carbamate[25] and imine groups.[26,27]

Using light to trigger the degradation of particles is particularly attractive owing to its noninvasive nature and facile spatiotemporal control. Recently, Shea and co-workers[28,29] have reported the use of a light-responsive coumarin-dimer bis-alkoxysilane to prepare thin films for photo-patterning applications. Inspired by this work, we have designed a new bis-alkoxysilane **1** (Figure 1) to be used as

the bridging organic moiety in the preparation of light-degradable mesoporous organosilica particles.
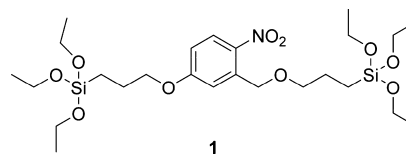
Figure 1. Molecular structure of photolabile bis-alkoxysilane **1**.

The photolabile moiety is a 2-nitrobenzyl ether group, which is known to undergo a Norrish type II reaction upon UV-light irradiation[30] that leads to its cleavage. Hence, when the linker is embedded in the silica framework, its light instability leads to the particle structural breakdown. The choice of the 2-nitrobenzyl derivative as a light-cleavable linker was based on its well-characterized photochemical properties. In fact, 2-nitrobenzyl derivatives have been used as caging groups for bioactive molecules,[31−33] as photoresponsive pore gatekeepers for controlled drug release,[34−36] as photolabile protecting groups for synthetic purposes,[37,38] and for the preparation of light-addressable materials,[39−41] for instance, polymers,[42] hydrogels,[39] and monolayers for photolithography.[43] In addition, the absorption spectrum of the 2-nitrobenzyl group can be finely tuned by introducing specific substituents on the

aromatic ring, thereby rendering the bond cleavage possible at different wavelengths.[44] Notably, compared to other reported photolabile groups (e.g., coumarin and arylmethyl derivatives), the 2-nitrobenzyl moiety presents reduced steric hindrance, which may avoid the collapse of pores and the formation of a disordered mesostructure during the preparation of the particles.

Examples of photoresponsive silica-based systems have been reported to date. In particular, light-responsive colloidosomes[45] and gated mesoporous silica particles,[46] as well as silica-based photocaged drug carriers[47] and photoresponsive silsesquioxane nanoparticles,[48] have been described. However, to the best of our knowledge, there are currently no reports on light-breakable mesoporous organosilica particles containing a photocleavable molecule integrated in the silica network, in which the degradation is triggered by UV light.

Here, we report the synthesis and thorough photochemical characterization of a new photodegradable bis-alkoxysilane **1** and its use for the preparation of light-breakable organo-bridged mesoporous silica particles (**LB-MSPs**). The particles have been characterized by several techniques and their degradation behavior upon UV-light exposure has been investigated. To demonstrate the applicability of **LB-MSPs** as porous containers for the light-stimulated release of a cargo molecule, the particles were loaded with 7-dehydrocholesterol, which is a natural vitamin D_3 precursor, and the triggered release of this molecule upon UV-light exposure was investigated.

2. EXPERIMENTAL SECTION

2.1. Synthesis of Alkoxysilane 1. *General Information.* Compound **1** was prepared according to the reactions shown in Scheme 1. All reactions were carried out under argon atmosphere.

Scheme 1. Synthesis of Photolabile Bis-alkoxysilane 1[a]
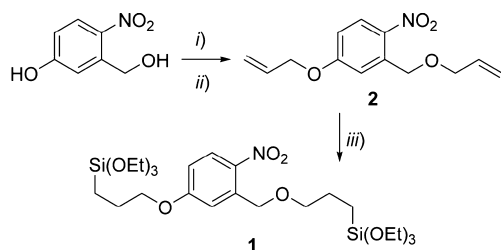
[a]Reaction conditions: (i) NaH, DMF, 0 °C; (ii) allylbromide, DMF, 0 °C to r.t.; (iii) Karstedt's catalyst, triethoxysilane, toluene, 50 °C.

The round-bottom flasks used in the reactions were oven-dried at 110 °C prior to use. All reactions were performed in anhydrous solvents as purchased from Sigma-Aldrich. The reaction progress was monitored by thin-layer chromatography (TLC) with silica gel 60 F_{254} coated on aluminum sheets (Merck). Flash column chromatography was carried out using 60−200 μm silica gel (VWR Chemicals). The solvents used were reagent grade or higher, unless otherwise noted. The following compounds were purchased from the listed supplies at the given purity and were used without further purification: sodium hydride (NaH, Sigma-Aldrich, 90%), 5-hydroxy-2-nitrobenzyl alcohol (Sigma-Aldrich, 97%), N,N-dimethylformamide (DMF, Sigma-Aldrich, anhydrous, 99.8%), triethoxysilane (Sigma-Aldrich, 95%), platinum(0)-1,3-diviynl-1,1,3,3-tetramethyldisiloxane complex solution (Karstedt's catalyst, Pt ∼ 2 wt % in xylene, Sigma-Aldrich), sodium sulfate (anhydrous, Sigma-Aldrich, ACS reagent), and sodium hydrogen carbonate (Sigma-Aldrich, ACS reagent >99.7%).

Synthesis of Compound 2. NaH (311 mg, 12.98 mmol) was added portion-wise to a stirring solution of 5-hydroxy-2-nitrobenzyl alcohol (1.00 g, 5.91 mmol) in dry DMF (10 mL) at 0 °C. After the completed addition of NaH, the reaction mixture was further stirred for 10 min at 0 °C. Subsequently, allyl bromide (1.17 mL, 13.52 mmol) was added dropwise to the stirring reaction mixture at 0 °C. The reaction mixture was stirred for 1 h at 0 °C and for a further 1 h at room temperature and was then quenched with water (5 mL). The aqueous layer was extracted with ethyl acetate (3×, 20 mL), and the combined organic layers were washed with a saturated Na_2CO_3 solution and brine and finally dried over anhydrous Na_2SO_4. Subsequently, the solvent was evaporated under reduced pressure and the crude oil was purified by column chromatography (silica gel, EtOAc/cyclohexane = 1:2), giving the diallyl intermediate **2** as a yellowish oil (1.05 g, 71%). ^1H NMR (CDCl$_3$, 400 MHz): δ 8.16 (d, 1H, J = 9.1 Hz), 7.37 (m, 1H), 6.87 (m, 1H), 6.09−5.94 (m, 2H), 5.47−5.23 (m, 4H), 4.94 (s, 2H), 4.66−4.64 (m, 2H), 4.17−4.15 (m, 2H) ppm. $^{13}C\{^1H\}$ NMR (CDCl$_3$, 100 MHz): δ 163.1, 139.8, 139.0, 134.2, 132.0, 127.6, 118.6, 117.3, 113.5, 113.3, 71.9, 69.3, 69.0 ppm. ATR-FTI $\tilde{\nu}_{max}$ [cm^{-1}]: 3861, 2854, 1577, 1508, 1336, 1321, 1282, 1228, 1066, 993, 923, 842, 754. HR-MS (ESI-TOF): m/z [M + H]$^+$ calcd for $C_{13}H_{16}NO_4$, 250.1079; found, 250.1073.

Synthesis of Compound 1. To a solution of **2** (1.00 g, 4.01 mmol) in dry toluene (9 mL), triethoxysilane (2.02 mL, 10.95 mmol) and subsequently platinum(0)-1,3-divinyl-1,1,3,3-tetramethyldisiloxane complex solution (Karstedt's catalyst, Pt ∼ 2 wt % in xylene, 125 μL) was added dropwise. The reaction mixture was stirred at 50 °C for 12 h. Additional Karstedt's catalyst solution (100 μL) was added, and the reaction mixture was stirred for a further 12 h at 50 °C. The organic solvent was evaporated under reduced pressure, and the crude oil was purified by column chromatography (silica gel, EtOAc/cyclohexane = 1:7), yielding compound **1** as a yellowish oil (692 mg, 63%). ^1H NMR (400 MHz, CDCl$_3$): δ 8.14 (d, 1H, J = 9.1 Hz), 7.31 (m, 1H), 6.83 (m, 1H), 4.90 (s, 2H), 4.04 (t, 2H, J = 6.7 Hz), 3.86−3.81 (m, 12H), 3.58 (t, 2H, J = 6.8 Hz), 1.97−1.90 (m, 2H), 1.84−1.77 (m, 2H), 1.23 (t, 18H, J = 7.0 Hz), 0.79−0.75 (m, 2H), 0.73−0.69 (m, 2H) ppm. $^{13}C\{^1H\}$ NMR (CDCl$_3$, 100 MHz): δ 163.3, 139.6, 139.3, 127.5, 113.3, 112.7, 73.5, 70.5, 69.6, 58.48, 58.41, 23.1, 22.6, 18.3, 6.6, 6.5 ppm. FTIR $\tilde{\nu}_{max}$[cm^{-1}]: 3016, 2978, 2931, 2889, 1583, 1512, 1442, 1388, 1340, 1323, 1286, 1230, 1165, 1103, 1078, 958. HR-MS (ESI-TOF): m/z [M + Na]$^+$ calcd for $C_{25}H_{47}NO_{10}Si_2Na$, 600.2636; found, 600.2624.

2.2. Preparation of LB-MSPs. *General Information.* The reaction was carried out in a 100 mL round-bottom flask equipped with a magnetic stirring bar (1 cm Teflon-coated cylindrical bar). EtOH from Carlo Erba (Analysis ACS-Reagent), hexadecyltrimethyl-lammonium bromide (CTAB, Acros Organics, 99+%), ammonia solution (VWR, 28%), tetraethyl orthosilicate (TEOS, Sigma-Aldrich, ≥99% GC), and bis[3-(triethoxysilyl)propyl]disulfide (fluorochem, tech grade) were used for the preparation of the particles.

Preparation of LB-MSPs. CTAB (50 mg, 0.137 mmol) was dissolved in an EtOH/H$_2$O mixture (14.5/30, v/v) and stirred at 250 rpm until its complete dissolution. Subsequently, NH$_3$ (28 wt %, 350 μL) was added to the stirring solution, and the stirring speed was increased to 1000 rpm. A mixture of TEOS (87.3 μL, 0.39 mmol) and compound **1** (100 mg, 0.173 mmol) in EtOH (500 μL) was added, and the mixture was stirred (1000 rpm) at r.t. overnight in the dark. The solution was decanted, leaving behind any material which was adhered to the walls, and the particles were recovered by centrifugation at 20 000 × g (15 min). Subsequent purification and extraction steps were carried out under the exclusion of light. Particles were thoroughly washed by sonication and centrifugation with distilled H$_2$O/EtOH (1:1, v/v; 2×) and EtOH (2×). The organic template was removed by refluxing the particles in EtOH for 12 h. The material was recovered by centrifugation, redispersed in EtOH, sonicated for 2 min, and centrifuged again. The particles were then refluxed for a further 12 h in EtOH and finally centrifuged, washed with EtOH (3×), and dried overnight under reduced pressure.
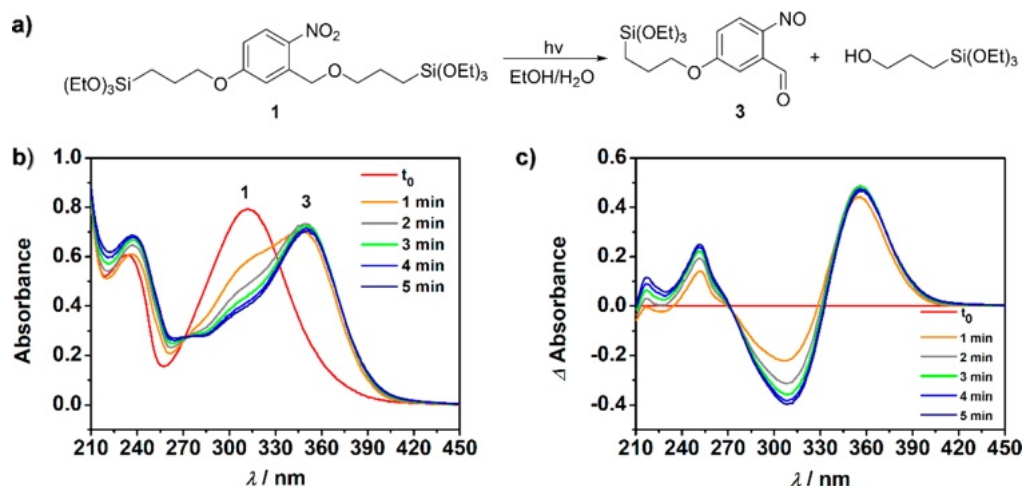
Figure 2. (a) Photodegradation reaction of compound **1**. (b) UV−vis absorption spectra of a 0.11 mM solution of **1** in EtOH/H₂O (5:1, *v/v*) recorded over time upon irradiation at 320 nm. (c) Difference absorbance spectra reported to visualize the spectral evolution.

3. RESULTS AND DISCUSSION

3.1. Synthesis and Characterization of the New Photolabile Alkoxysilane. Compound **1** was synthesized according to the synthetic path depicted in Scheme 1 (see Experimental Section for details on syntheses and characterization; NMR spectra are reported in the Supporting Information). As the first step, 5-hydroxy-2-nitrobenzyl alcohol was reacted with allyl bromide by using sodium hydride as the base, giving the diallyl ether compound **2** with a good yield. Subsequent hydrosilylation of **2** with triethoxysilane in the presence of Karstedt's catalyst afforded the final compound **1**. The compounds were characterized by ¹H and ¹³C NMR spectroscopy (spectra are reported in Figures S1−S4), Fourier transform infrared spectroscopy (FTIR; Figure S5), and mass spectrometry.

As discussed in the introduction, the photodegradable 2-nitrobenzyl ether moiety is known to undergo the Norrish type II reaction under UV-light irradiation, which leads to its specific O_{bz}−C bond cleavage (Figure 2a).[49] Therefore, embedding alkoxysilane **1** in the silica framework should lead to the structural breakdown of particles upon UV-light exposure. Light-degradation studies were performed through UV−vis and ¹H NMR spectroscopy to determine the minimum wavelength of light required to trigger degradation of **1** and to follow its degradation path.

The UV−vis absorption spectrum of **1** (0.11 mM) in a mixture EtOH/H₂O (5:1, v/v; Figure 2a, profile corresponding to t_0) showed the characteristic absorption band of the n−π* transition centered at 312 nm. The solution was then irradiated at 320 nm (see Supporting Information for experimental details), and UV−vis absorption spectra were recorded over time (Figure 2b). The profile evolution shows a decrease in intensity of the absorption band at 312 nm, which was completely absent already after the first 5 min of irradiation, whereas a new n−π* transition band at 352 nm appeared, indicating the fast formation of the nitrosobenzaldehyde degradation product **3** (Figure 2b), which is in agreement with results on similar compounds reported in the literature.[49] The solvent mixture composed of EtOH and water was chosen because the photodegradation of 2-nitrobenzyl ethers is known to be accelerated by the presence of water.[49] However, a high EtOH/H₂O ratio was chosen and water was used only in a relatively small percentage to avoid, in the case of the

organosilica nanoparticles, degradation of silica particles induced by hydrolysis.

The formation of the nitrosobenzaldehyde degradation product **3** was further supported by time-dependent density functional theory (TD-DFT, see Supporting Information for details). The calculated UV−vis absorption spectrum of a nitroso model structure showed good agreement with the spectrum observed after the exposure of **1** to 30 min of UV-light irradiation (Figure S7).

The cleavage of the benzylic ether was further confirmed by the ¹H NMR spectra (see Supporting Information for details) of the sample at different time intervals upon irradiation of a solution, in deuterated solvent, of **1** at 320 nm (Figure S6). The photodegradation was proven by the appearance of the aldehyde −C*H*O signal at 10.49 ppm and the decrease in intensity of both the singlet signal of the benzylic −CH₂− signal at 4.89 ppm and the triplet signal, attributed to the −$O_{bz}CH_2CH_2$− of the aliphatic chain, at 3.57 ppm. The decay of the benzylic −C*H₂*− signal was subsequently used to determine the reaction quantum yield, Φ_{365}, for the degradation process through a previously reported NMR-based chemical actinometry method (see Supporting Information for details).[50,51] These studies were performed by using >60 mM solutions of **1** in CDCl₃ placed in quartz NMR tubes. CDCl₃ was used to avoid the presence of water, which could cause the alkoxysilane hydrolysis in the time range of the measurement. Irradiation of the **1** solution, in the NMR tube with an intensity-calibrated 365 nm LED, shows the decay of the benzylic peak as a function of irradiation time. The decay of this peak was used to quantify the change in concentration as a function of time, and the resulting concentration vs irradiation time plot was fit to a first order kinetic model in order to quantify the initial reaction rate (k_0) (Figures S8 and S9). The initial reaction rate was then used to determine a quantum yield of 0.30 ± 0.09 by using eq 1, in which I_0 is the intensity of the calibrated LED.

$$I_0 = \frac{k_0}{\phi_{365}} \tag{1}$$

3.2. Preparation of the Light-Breakable Mesoporous Organo-Bridged Silica Particles. Once the degradation of the alkoxysilane **1** upon UV-light exposure had been assessed,
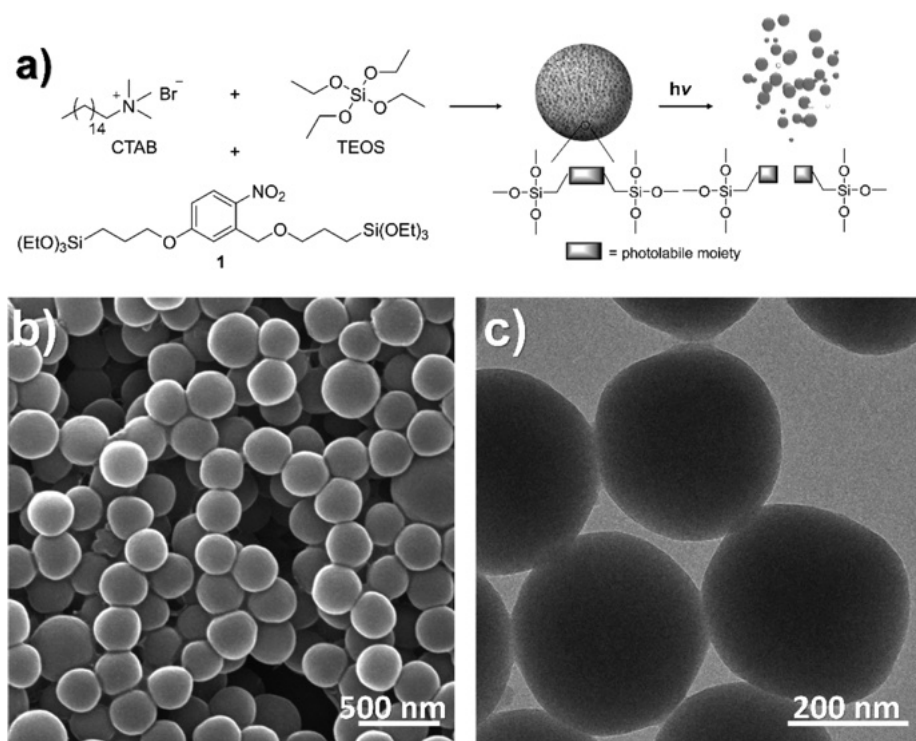
Figure 3. (a) Schematic representation of the preparation and light-induced degradation of **LB-MSPs**. (b) SEM and (c) TEM images of **LB-MSPs**.

the compound was used to prepare **LB-MSPs**. As depicted in Figure 3a, the **LB-MSPs** were prepared by modifying a recently reported procedure for the preparation of pristine 200 nm silica nanoparticles.[27] In this modified Stöber process,[52] the photolabile linker **1** was co-condensed to tetraethyl orthosilicate (TEOS), by using a molar ratio TEOS/**1** 2.25:1, in the presence of CTAB as the organic template and aqueous NH_3 as the basic catalyst. The reaction was performed in the dark to prevent photodegradation of **1**. The particles were recovered by centrifugation, and the surfactant was removed upon extraction in EtOH at 80 °C for 24 h in the dark (see Supporting Information for further details).

Initial morphological characterization was first performed by scanning electron microscopy (SEM, Figure 3b), which revealed the formation of spherical particles characterized by an average size of 303 ± 34 nm (Figure S10). Dynamic light scattering measurements (DLS, Figure S11) on a dispersion of **LB-MSPs** in EtOH gave a hydrodynamic diameter (D_h) of 409 ± 80 nm, showing a good dispersibility of the particles. Transmission electron microscopy (TEM, Figures 3c and S26) confirmed both particle morphology and size. In addition, no ordered array of pores was observed, suggesting that the introduction of the bulky linker affects the mesostructure, resulting in a decreased mesopore order in **LB-MSPs**.

N_2 adsorption−desorption measurements revealed the presence of pores characterized by an average width of 2.4 nm (Figure 4a), with a total pore volume of 0.26 cm³/g and BET specific surface area of 318 m²/g. The small-angle X-ray scattering (SAXS) pattern showed two very broad peaks of low intensity centered at q = 1.8 and 2.9 nm^{-1} (Figure S12), indicating the presence of a nonordered porous structure, in agreement with TEM observations. The amount of organic linker in **LB-MSPs** was quantified by thermogravimetric analysis (TGA). The thermograms of both **1** and **LB-MSPs** are displayed in Figure 4b showing that the organic content in
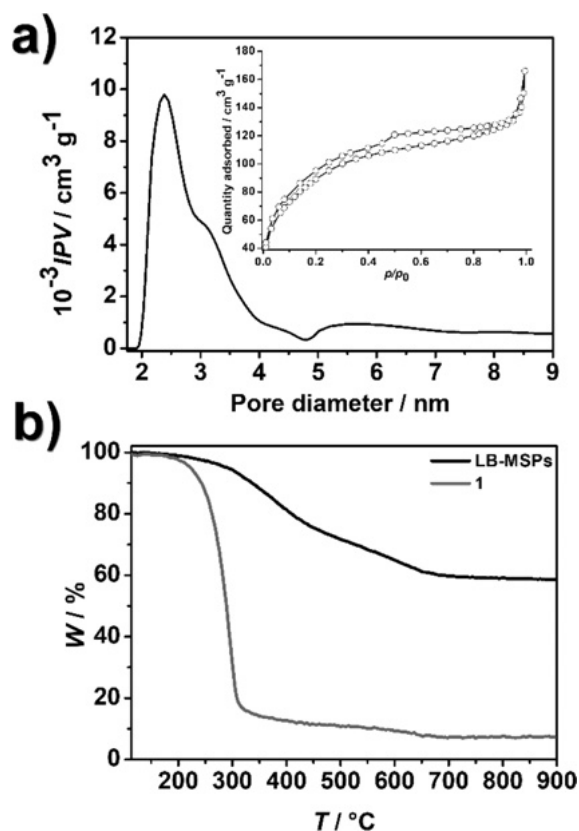
Figure 4. (a) Pore size distribution of **LB-MSPs** calculated from the N_2 adsorption branch; adsorption−desorption isotherms are reported in the inset. (b) Thermograms recorded on **LB-MSPs** (black line) and compound **1** (gray line).
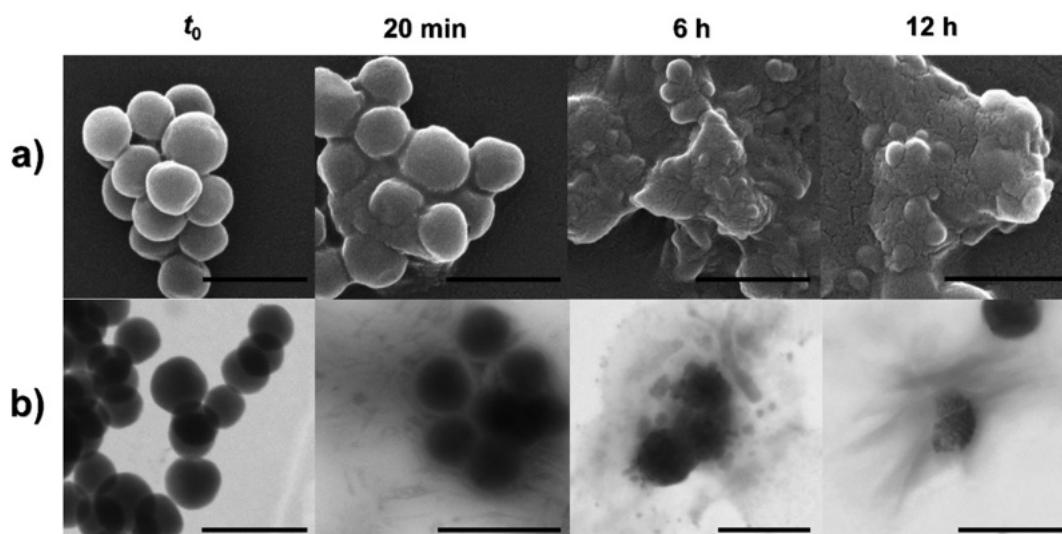
Figure 5. (a) SEM and (b) STEM images of **LB-MSPs** at t_0 and after 20 min and 6 h of UV-light irradiation at 327 nm, scale bar = 500 nm.

the particles is around 30 wt %. This loss was attributed to the organic linker **1** based on the weight loss observed for pristine mesoporous silica particles (**MSPs**) prepared under analogous conditions (Figure S13; see ref 27 for preparation details).

The integration of the photolabile linker into the mesoporous structure was demonstrated by means of attenuated total reflectance Fourier transform infrared spectroscopy (ATR-FTIR) and X-ray photoelectron spectroscopy (XPS). The ATR-FTIR spectrum recorded on **LB-MSPs** (Figure S14) showed bands at 1512 and 1340 cm^{-1} that are typical of $-NO_2$ stretching modes, the aromatic C=C stretching bands at 1610 and 1583 cm^{-1}, and the $C_{sp2}-H$ and $C_{sp3}-H-$ stretching vibrations at 3016, 2978, 2929, and 2887 cm^{-1}, which are not present in the spectrum of pristine **MSPs** (see Supporting Information for further details).[53] Further confirmation of the presence of the organic linker was given by the XPS analysis. The survey spectrum recorded on the **LB-MSPs** (Figure S15a) revealed the presence of C(1s) and N(1s) signals at 285 and 405 eV, respectively. Moreover, the high resolution (HR) scans of C(1s) and N(1s) core levels clearly confirm the presence of the linker within the silica structure. The deconvolution of the HR scan for the N(1s) peak (Figure S15c) shows the presence of two components, N-1 at 405.6 eV and N-2 at 400.2 eV, in a ratio (area) of 3.6:1. The component N-1 is attributable to the nitrogen of the aromatic NO_2 group, whereas the N-2 component is attributable to the nitrogen of the NO group, which is probably formed on the surface of the particle upon exposure to light during the sample preparation. The analysis of the HR scan of the C(1s) core level (Figure S15b) demonstrated the presence of three components C-1 (285.9 eV), C-2 (284.8 eV), and C-3 (284.1 eV) that can be attributed to $C-O$, $C-C$, and aromatic C, respectively. The attribution of signals was performed in agreement with data reported in the literature.[54] Finally, the UV−vis absorption spectrum of **LB-MSPs** showed two characteristic absorption bands with a maximum in absorbance at 242 and 327 nm, which can be attributed to the presence of **1** in the silica framework (Figure S16).

3.3. Light-Triggered Degradation of LB-MSPs.
To assess the ability of **LB-MSPs** to break upon exposure to UV light, a particle dispersion (0.1 mg/mL in a 5:1 (v/v) EtOH/ H$_2$O mixture) was irradiated at λ = 327 nm and the system

evolution was followed by SEM, STEM, and UV−vis absorption spectroscopy. This wavelength was selected due to the observed bathochromic shift of the maximum absorption wavelength of **1** from 320 to 327 nm, upon integration into the silica structure. As shown in the SEM images (Figure 5a), the surfaces of particles became rougher after 20 min of UV-light exposure and amorphous material was present, most probably due to particle degradation. Prolonged light irradiation led to an enhanced structural breakdown of **LB-MSPs**, as demonstrated by complete loss of their initial morphology after 6 h of light exposure. The particles degraded, forming small debris that could be observed as aggregates, likely due to a drying effect on the glass coverslip occurring during SEM sample preparation (Figure 5a, 6 and 12 h). The STEM images (Figure 5b) recorded on the same sample further confirmed particle degradation into small debris. Particles with reduced core densities were not observed during the degradation process, suggesting that degradation occurs from the exterior of the particle. UV−vis absorption spectra recorded over time on the **LB-MSPs** dispersion (Figure 6) confirmed that the degradation is triggered by the cleavage of the photolabile moiety. After 20 min of irradiation the absorbance feature at 327 nm, attributed to the linker **1**, was absent, thereby indicating its photodegradation. This spectral evolution over time upon light irradiation is in agreement with the results obtained for the linker **1** alone. To verify that no
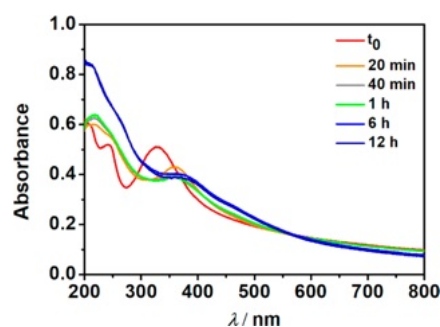
Figure 6. UV−vis absorption spectra recorded over time on a dispersion of **LB-MSPs** in EtOH/H$_2$O (5:1, v/v) upon light irradiation at λ = 327 nm.

dissolution of **LB-MSPs** was occurring in the same time range without light exposure, a control experiment was performed keeping the **LB-MSPs** dispersion in the dark and analyzing aliquots over time. As reported in Figure S17, the particles did not show any appreciable change in morphology and the characteristic UV−vis absorption spectra attributable to **1** was preserved, demonstrating that **LB-MSPs** are stable in these conditions and that their degradation can only be attributed to the effect of UV-light irradiation.

As a further proof of the particle degradation, we performed N_2 sorption analysis on irradiated **LB-MSPs**. A suspension of **LB-MSPs** in $EtOH/H_2O$ (5:1, v/v) was irradiated for 24 h, and then the solvent was removed by freeze-drying and the resulting powder used for the measurement. As depicted in Figure S18, the amount of adsorbed N_2 is significantly reduced, and the calculated total pore volume and the BET specific surface areas for the irradiated particles are substantially decreased to 0.03 cm^3/g and 57 m^2/g, respectively. This clearly indicates a decrease of porosity, confirming the degradation of the material.

Furthermore, considering a potential use of **LB-MSPs** in biorelated applications, we performed a preliminary biological study, in which the cytocompatibilities of the particle and of their degradation products were assessed. HeLa cells were therefore incubated with either pristine **LB-MSPs** or particles that had been previously exposed to 12 h of UV-light irradiation (**LB-MSPs-irr**; for details see the Methods section, Supporting Information). The cells were incubated for 12 and 24 h with **LB-MSPs** and **LB-MSPs-irr** at three different concentrations (20, 100, 200 $\mu g/mL$), and the cell viability was determined by using the Alamar Blue assay. As shown in Figure S19, no significant cytotoxicity was observed in this range of concentrations and over the monitored period.

3.4. Release Study. Once the effective light-induced degradation of **LB-MSPs** was proven, we verified whether the particles could serve as potential responsive delivery vehicles for stimuli-triggered and enhanced release of molecules. Therefore, **LB-MSPs** were loaded with 7-dehydrocholesterol (**7-DH**, see Supporting Information for details), a hydrophobic test molecule of biological interest, which is a natural vitamin D3 precursor. The release of the hydrophobic cargo with and without irradiation was monitored by UV−vis absorption spectroscopy.

To load **7-DH**, the particles were suspended in a highly concentrated solution (20 mg/mL) of the molecule in ethanol and stirred for 24 h. After evaporation of the solvent, the particles were washed with a $H_2O/EtOH$ (9:1, v/v) mixture and then dried under reduced pressure (see Supporting Information for further details). The final loading was determined to be 23 wt % by TGA (Figure S20). The release of **7-DH** was monitored by modifying a previously reported method.[20] Briefly, an aqueous particle dispersion (0.78 mg mL^{-1}) was prepared, and 500 μL were placed in a 10 mm path length quartz cuvette equipped with a small stirring bar. A layer of cyclohexane (2 mL) was then added on top of the aqueous particle dispersion to extract the hydrophobic compound. Under gentle stirring, avoiding the mixing of the two separate phases, the aqueous suspension was irradiated at 327 nm and the variation of absorbance at λ_{max} = 281 nm in the upper organic phase was monitored over time (see Supporting Information for further details).

A boosted release of **7-DH** upon UV-light irradiation was observed, which can be explained by the enhanced disruption

of **LB-MSPs** once exposed to light, whereas in the absence of light only a lower amount of **7-DH** was released most probably due to the passive diffusion of the molecule loaded in the pores or physisorbed onto the particle surface (Figure 7 and Figure
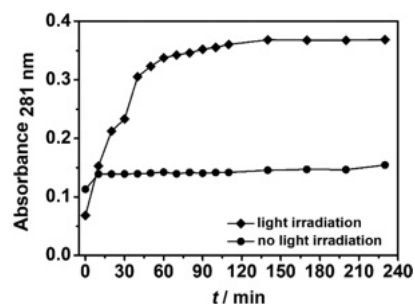
Figure 7. Release of **7-DH** from **LB-MSPs** upon UV-light irradiation at λ = 327 nm and without irradiation. The **7-DH** release was investigated by monitoring the variation of absorbance at λ = 281 nm.

S21a,b). The amount of **7-DH** released could be estimated from the calibration curve obtained for **7-DH** in the same solvent (Figure S21c). Considering the amount of **LB-MSPs** used and the **7-DH** loading of 23 wt %, a 3-fold release of **7-DH** upon light exposure of **LB-MSPs**, compared to particles stirred in the dark, was observed.

To further confirm that the release of **7-DH** is only triggered by light, we performed the same experiment by using as reference materials pristine mesoporous silica particles (**MSPs**) and disulfide-bridged mesoporous silica particles (**SS-MSPs**), that is, particles containing an organic linker which cannot be cleaved upon UV-light exposure. While we have previously reported the preparation and characterization of **MSPs**,[27] **SS-MSPs** of size and physicochemical properties comparable to those of **LB-MSPs** were prepared anew; the preparation was performed by modifying the protocol used to obtain **LB-MSPs** (see Supporting Information, Methods section, for details, and Figure S22 for characterization). The reference particles were loaded with **7-DH** following the same procedure used for **LB-MSPs**, and their was loading determined by TGA (Figures S22d and 23; section Methods in the Supporting Information). The release experiments showed (Figure S24) that, besides the passive diffusion of the cargo molecule, no enhanced release was observed from **MSPs** and **SS-MSPs** when irradiated at 327 nm, confirming that the release observed for **LB-MSPs** is exclusively due to the photodegradation occurring upon exposure to light. Finally, to support these results and further exclude that the release of **7-DH** could be due to a thermic effect, we irradiated the loaded particles at 500 nm, that is, at a wavelength at which the photodegradable linker does not degrade. Figure S25 shows that, upon 500 nm light irradiation, no enhanced **7-DH** release can be observed in addition to the fast passive diffusion of physisorbed molecules, and that the triggered enhanced release can be observed only once the wavelength of the irradiation light is switched to 327 nm.

4. CONCLUSIONS

In summary, we have presented for the first time the preparation and characterization of spherical mesoporous organosilica particles that degrade upon UV-light irradiation. The particles, **LB-MSPs**, were prepared by co-condensation with TEOS with a new light-cleavable bis-alkoxysilane, bearing the photolabile 2-nitrobenzyl ether functional group. The

cleavage of the linker takes place upon UV-light irradiation and with a reaction quantum yield of 0.30 ± 0.09. Incorporation of the linker in the silica framework yielded light-responsive particles that showed signs of degradation after only 20 min of exposure to UV light. The particles have been employed as light-responsive containers for the boosted release of provitamin D_3 (7-dehydrocholesterol), which was observed upon UV-light irradiation. This work demonstrates that also a physical triggering stimulus can be employed to obtain silica-based responsive materials. The stability in the dark of the system and the enhanced degradation in the presence of light open new possibilities in the design of a caged system able to release hydrophobic molecules.

■ ASSOCIATED CONTENT

ⓢ Supporting Information

The Supporting Information is available free of charge at https://pubs.acs.org/doi/10.1021/acs.chemmater.9b03937.

> Experimental details and description of materials and instruments as well as additional figures (PDF)

■ AUTHOR INFORMATION

Corresponding Authors
*(L.T.) E-mail: l.trvgln@gmail.com.
*(L.D.C.) E-mail: decola@unistra.fr.
ORCID ⓘ
M. Carmen Ortega-Liebana: 0000-0001-5835-1223
Luisa De Cola: 0000-0002-2152-6517
Notes
The authors declare no competing financial interest.

■ ACKNOWLEDGMENTS

■ REFERENCES

(1) Ishikawa, S.; Maegawa, Y.; Waki, M.; Inagaki, S. Immobilization of a Molybdenum Complex on Bipyridine-Based Periodic Mesoporous Organosilica and Its Catalytic Activity for Epoxidation of Olefins. *ACS Catal.* **2018**, *8* (5), 4160−4169.

(2) Waki, M.; Yamanaka, K. I.; Shirai, S.; Maegawa, Y.; Goto, Y.; Yamada, Y.; Inagaki, S. Re(Bpy)(CO)$_3$Cl Immobilized on Bipyridine-Periodic Mesoporous Organosilica for Photocatalytic CO$_2$Reduction. *Chem. - Eur. J.* **2018**, *24* (15), 3846−3853.

(3) Ouwehand, J.; Lauwaert, J.; Esquivel, D.; Hendrickx, K.; Van Speybroeck, V.; Thybaut, J. W.; Van Der Voort, P. Facile Synthesis of Cooperative Acid-Base Catalysts by Clicking Cysteine and Cysteamine on an Ethylene-Bridged Periodic Mesoporous Organosilica. *Eur. J. Inorg. Chem.* **2016**, *2016* (13−14), 2144−2151.

(4) Yang, Q.; Liu, J.; Zhang, L.; Li, C. Functionalized Periodic Mesoporous Organosilicas for Catalysis. *J. Mater. Chem.* **2009**, *19* (14), 1945−1955.

(5) Dreifke, M.; Brieler, F. J.; Fröba, M. Immobilization of Alcohol Dehydrogenase from E. Coli onto Mesoporous Silica for Application as a Cofactor Recycling System. *ChemCatChem* **2017**, *9* (7), 1148.

(6) Sanchez, C.; Jeremias, F.; Ernst, S. J.; Henninger, S. K. Synthesis, Functionalization and Evaluation of Ethylene-Bridged PMOs as Adsorbents for Sorption Dehumidification and Cooling Systems. *Microporous Mesoporous Mater.* **2017**, *244*, 151−157.

(7) Lee, S. H.; Park, S. S.; Parambadath, S.; Ha, C. S. Sulphonic Acid Functionalized Periodic Mesoporous Organosilica with the Bridged Bissilylated Urea Groups for High Selective Adsorption of Cobalt Ion

from Artificial Seawater. *Microporous Mesoporous Mater.* **2016**, *226*, 179−190.

(8) Esquivel, D.; Ouwehand, J.; Meledina, M.; Turner, S.; Van Tendeloo, G.; Romero-Salguero, F. J.; Clercq, J. De; Van Der Voort, P. Thiol-Ethylene Bridged PMO: A High Capacity Regenerable Mercury Adsorbent via Intrapore Mercury Thiolate Crystal Formation. *J. Hazard. Mater.* **2017**, *339*, 368−377.

(9) Chen, F.; Zhao, E.; Kim, T.; Wang, J.; Hableel, G.; Reardon, P. J. T.; Ananthakrishna, S. J.; Wang, T.; Arconada-Alvarez, S.; Knowles, J. C.; Jokerst, J. V. Organosilica Nanoparticles with an Intrinsic Secondary Amine: An Efficient and Reusable Adsorbent for Dyes. *ACS Appl. Mater. Interfaces* **2017**, *9* (18), 15566−15576.

(10) Morante-Zarcero, S.; Pérez-Quintanilla, D.; Sierra, I. A Disposable Electrochemical Sensor Based on Bifunctional Periodic Mesoporous Organosilica for the Determination of Lead in Drinking Waters. *J. Solid State Electrochem.* **2015**, *19* (7), 2117−2127.

(11) Lu, D.; Chen, H.; Yan, X.; Wang, L.; Zhang, J. Ratiometric Hg2+ Sensor Based on Periodic Mesoporous Organosilica Nanoparticles and Förster Resonance Energy Transfer. *J. Photochem. Photobiol., A* **2015**, *299*, 125−130.

(12) Du, X.; Li, X.; Xiong, L.; Zhang, X.; Kleitz, F.; Qiao, S. Z. Mesoporous Silica Nanoparticles with Organo-Bridged Silsesquioxane Framework as Innovative Platforms for Bioimaging and Therapeutic Agent Delivery. *Biomaterials* **2016**, *91*, 90−127.

(13) Yu, L.; Chen, Y.; Lin, H.; Du, W.; Chen, H.; Shi, J. Ultrasmall Mesoporous Organosilica Nanoparticles: Morphology Modulations and Redox-Responsive Biodegradability for Tumor-Specific Drug Delivery. *Biomaterials* **2018**, *161*, 292−305.

(14) Croissant, J. G.; Zink, J. I.; Raehm, L.; Durand, J. Two-Photon-Excited Silica and Organosilica Nanoparticles for Spatiotemporal Cancer Treatment. *Adv. Healthcare Mater.* **2018**, *7*, 1701248.

(15) Croissant, J. G.; Fatieiev, Y.; Omar, H.; Anjum, D. H.; Gurinov, A.; Lu, J.; Tamanoi, F.; Zink, J. I.; Khashab, N. M. Periodic Mesoporous Organosilica Nanoparticles with Controlled Morphologies and High Drug/Dye Loadings for Multicargo Delivery in Cancer Cells. *Chem. - Eur. J.* **2016**, *22* (28), 9607−9615.

(16) Lu, N.; Fan, W.; Yi, X.; Wang, S.; Wang, Z.; Tian, R.; Jacobson, O.; Liu, Y.; Yung, B. C.; Zhang, G.; et al. Biodegradable Hollow Mesoporous Organosilica Nanotheranostics for Mild Hyperthermia-Induced Bubble-Enhanced Oxygen-Sensitized Radiotherapy. *ACS Nano* **2018**, *12* (2), 1580−1591.

(17) Croissant, J. G.; Fatieiev, Y.; Almalik, A.; Khashab, N. M. Mesoporous Silica and Organosilica Nanoparticles: Physical Chemistry, Biosafety, Delivery Strategies, and Biomedical Applications. *Adv. Healthcare Mater.* **2018**, *7* (4), 1700831.

(18) Croissant, J. G.; Fatieiev, Y.; Khashab, N. M. Degradability and Clearance of Silicon, Organosilica, Silsesquioxane, Silica Mixed Oxide, and Mesoporous Silica Nanoparticles. *Adv. Mater.* **2017**, *29* (9), 1604634.

(19) Croissant, J.; Cattoën, X.; Man, M. W. C.; Gallud, A.; Raehm, L.; Trens, P.; Maynadier, M.; Durand, J. O. Biodegradable Ethylene-Bis(Propyl)Disulfide-Based Periodic Mesoporous Organosilica Nanorods and Nanospheres for Efficient in-Vitro Drug Delivery. *Adv. Mater.* **2014**, *26* (35), 6174−6180.

(20) Maggini, L.; Cabrera, I.; Ruiz-Carretero, A.; Prasetyanto, E. A.; Robinet, E.; De Cola, L. Breakable Mesoporous Silica Nanoparticles for Targeted Drug Delivery. *Nanoscale* **2016**, *8* (13), 7240−7247.

(21) Du, X.; Kleitz, F.; Li, X.; Huang, H.; Zhang, X.; Qiao, S. Z. Disulfide-Bridged Organosilica Frameworks: Designed, Synthesis, Redox-Triggered Biodegradation, and Nanobiomedical Applications. *Adv. Funct. Mater.* **2018**, *28* (26), 1707325.

(22) Shao, D.; Li, M.; Wang, Z.; Zheng, X.; Lao, Y. H.; Chang, Z.; Zhang, F.; Lu, M.; Yue, J.; Hu, H.; et al. Bioinspired Diselenide-Bridged Mesoporous Silica Nanoparticles for Dual-Responsive Protein Delivery. *Adv. Mater.* **2018**, *30* (29), 1801198.

(23) Fatieiev, Y.; Croissant, J. G.; Julfakyan, K.; Deng, L.; Anjum, D. H.; Gurinov, A.; Khashab, N. M. Enzymatically Degradable Hybrid Organic-inorganic Bridged Silsesquioxane Nanoparticles for in Vitro Imaging. *Nanoscale* **2015**, *7* (37), 15046−15050.

(24) Maggini, L.; Travaglini, L.; Cabrera, I.; Castro-Hartmann, P.; De Cola, L. Biodegradable Peptide-Silica Nanodonuts. *Chem. - Eur. J.* **2016**, *22* (11), 3697−3703.

(25) Gao, Z.; Hadipour Moghaddam, S. P.; Ghandehari, H.; Zharov, I. Synthesis of Water-Degradable Silica Nanoparticles from Carbamate-Containing Bridged Silsesquioxane. *RSC Adv.* **2018**, *8*, 4914−4920.

(26) Liu, L.; Kong, C.; Huo, M.; Liu, C.; Peng, L.; Zhao, T.; Wei, Y.; Qian, F.; Yuan, J. Schiff Base Interaction Tuned Mesoporous Organosilica Nanoplatforms with PH-Responsive Degradability for Efficient Anti-Cancer Drug Delivery: In Vivo. *Chem. Commun.* **2018**, *54* (66), 9190−9193.

(27) Travaglini, L.; Picchetti, P.; Totovao, R.; Prasetyanto, E. A.; De Cola, L. Highly Degradable Imine-Doped Mesoporous Silica Particles. *Mater. Chem. Front.* **2019**, *3* (1), 111−119.

(28) Zhao, L.; Vaupel, M.; Loy, D. A.; Shea, K. J. Photoresponsive Hybrid Materials: Synthesis and Characterization of Coumarin-Dimer-Bridged Polysilsesquioxanes. *Chem. Mater.* **2008**, *20* (5), 1870−1876.

(29) Zhao, L.; Loy, D. A.; Shea, K. J. Photodeformable Spherical Hybrid Nanoparticles. *J. Am. Chem. Soc.* **2006**, *128* (44), 14250−14251.

(30) Bochet, C. G. Photolabile Protecting Groups and Linkers. *J. Chem. Soc. Perkin Trans. 1* **2002**, *2*, 125−142.

(31) Pellois, J.-P.; Muir, T. W. A Ligation and Photorelease Strategy for the Temporal and Spatial Control of Protein Function in Living Cells. *Angew. Chem., Int. Ed.* **2005**, *44*, 5713−5717.

(32) Elamri, I.; Heumuller, M.; Herzig, L.-M.; Stirnal, E.; Wachtveitl, J.; Schuman, E. M.; Schwalbe, H. A New Photocaged Puromycin for an Efficient Labeling of Newly Translated Proteins in Living Neurons. *ChemBioChem* **2018**, *19*, 2458−2464.

(33) Lin, Y.; Mazo, M. M.; Skaalure, S. C.; Thomas, M. R.; Schultz, S. R.; Stevens, M. M. Activatable Cell-Biomaterial Interfacing with Photo-Caged Peptides. *Chem. Sci.* **2019**, *10*, 1158−1167.

(34) Park, C.; Lee, K.; Kim, C. Photoresponsive Cyclodextrin-Covered Nanocontainers and Their Sol-Gel Transition Induced by Molecular Recognition. *Angew. Chem., Int. Ed.* **2009**, *48* (7), 1275−1278.

(35) Lai, J.; Mu, X.; Xu, Y.; Wu, X.; Wu, C.; Li, C.; Chen, J.; Zhao, Y. Light-Responsive Nanogated Ensemble Based on Polymer Grafted Mesoporous Silica Hybrid Nanoparticles. *Chem. Commun.* **2010**, *46* (39), 7370.

(36) Zhu, J.; Niu, Y.; Li, Y.; Gong, Y.; Shi, H.; Huo, Q.; Liu, Y.; Xu, Q. Stimuli-Responsive Delivery Vehicles Based on Mesoporous Silica Nanoparticles: Recent Advances and Challenges. *J. Mater. Chem. B* **2017**, *5* (7), 1339−1352.

(37) Li, J.; Jeong, S.; Esser, L.; Harran, P. G. Total Synthesis of Nominal Diazonamides - Part 1: Convergent Preparation of the Structure Proposed for (-)-Diazonamide A. *Angew. Chem., Int. Ed.* **2001**, *40* (24), 4765−4769.

(38) Kessler, M.; Glatthar, R.; Giese, B.; Bochet, C. G. Sequentially Photocleavable Protecting Groups in Solid-Phase Synthesis. *Org. Lett.* **2003**, *5* (8), 1179−1181.

(39) Kloxin, A. M.; Kasko, A. M.; Salinas, C. N.; Anseth, K. S. Photodegradable Hydrogels for Dynamic Tuning of Physical and Chemical Properties. *Science* **2009**, *324*, 59−63.

(40) Fomina, N.; Mcfearin, C.; Sermsakdi, M.; Edigin, O.; Almutairi, A. UV and Near-IR Triggered Release from Polymeric Micelles and Nanoparticles. *J. Am. Chem. Soc.* **2010**, *132* (28), 9540−9542.

(41) Lunzer, M.; Shi, L.; Andriotis, O. G.; Gruber, P.; Markovic, M.; Thurner, P. J.; Ossipov, D.; Liska, R.; Ovsianikov, A. A Modular Approach to Sensitized Two-Photon Patterning of Photodegradable Hydrogels. *Angew. Chem., Int. Ed.* **2018**, *57* (46), 15122−15127.

(42) Roppolo, I.; Chiappone, A.; Angelini, A.; Stassi, S.; Frascella, F.; Pirri, C. F.; Ricciardi, C.; Descrovi, E. 3D Printable Light-Responsive Polymers. *Mater. Horiz.* **2017**, *4* (3), 396−401.

(43) Critchley, K.; Zhang, L.; Fukushima, H.; Ishida, M.; Shimoda, T.; Bushby, R. J.; Evans, S. D. Soft-UV Photolithography Using Self-Assembled Monolayers. *J. Phys. Chem. B* **2006**, *110* (34), 17167−17174.

(44) Hansen, M. J.; Velema, W. A.; Lerch, M. M.; Szymanski, W.; Feringa, B. L. Wavelength-Selective Cleavage of Photoprotecting Groups: Strategies and Applications in Dynamic Systems. *Chem. Soc. Rev.* **2015**, *44* (11), 3358−3377.

(45) Li, S.; Moosa, B. A.; Croissant, J. G.; Khashab, N. M. Electrostatic Assembly/Disassembly of Nanoscaled Colloidosomes for Light-Triggered Cargo Release. *Angew. Chem., Int. Ed.* **2015**, *54* (23), 6804−6808.

(46) He, D.; He, X.; Wang, K.; Cao, J.; Zhao, Y. A Light-Responsive Reversible Molecule-Gated System Using Thymine-Modified Mesoporous Silica Nanoparticles. *Langmuir* **2012**, *28* (8), 4003−4008.

(47) Lin, Q. N.; Huang, Q.; Li, C. Y.; Bao, C. Y.; Liu, Z. Z.; Li, F. Y.; Zhu, L. Y. Anticancer Drug Release from a Mesoporous Silica Based Nanophotocage Regulated by Either a One- or Two- Photon Process. *J. Am. Chem. Soc.* **2010**, *132*, 10645−10647.

(48) Fatieiev, Y.; Croissant, J. G.; Alsaiari, S.; Moosa, B. A.; Anjum, D. H.; Khashab, N. Photoresponsive Bridged Silsesquioxane Nanoparticles with Tunable Morphology for Light-Triggered Plasmid DNA Delivery. *ACS Appl. Mater. Interfaces* **2015**, *7*, 24993−24997.

(49) Il'ichev, Y. V.; Schworer, M. A.; Wirz, J. Photochemical Reaction Mechanisms of 2-Nitrobenzyl Compounds: Methyl Ethers and Caged ATP. *J. Am. Chem. Soc.* **2004**, *126*, 4581−4595.

(50) Willett, K. L.; Hites, R. A. Chemical Actinometry: Using o-Nitrobenzaldehyde to Measure Lamp Intensity in Photochemical Experiments. *J. Chem. Educ.* **2000**, *77* (7), 900−902.

(51) Ji, Y.; DiRocco, D. A.; Hong, C. M.; Wismer, M. K.; Reibarkh, M. Facile Quantum Yield Determination via NMR Actinometry. *Org. Lett.* **2018**, *20* (8), 2156−2159.

(52) Grün, M.; Lauer, I.; Unger, K. K. The Synthesis of Micrometer- and Submicrometer-Size Spheres of Ordered Mesoporous Oxide MCM-41. *Adv. Mater.* **1997**, *9* (3), 254−257.

(53) Dunkin, I. R.; Gębicki, J.; Kiszka, M.; Sanín-Leira, D. Phototautomerism of O-Nitrobenzyl Compounds: O-Quinonoid Aci-Nitro Species Studied by Matrix Isolation and DFT Calculations. *J. Chem. Soc. Perkin Trans. 2* **2001**, *8*, 1414−1425.

(54) Yang, G.; Hu, H.; Zhou, Y.; Hu, Y.; Huang, H.; Nie, F.; Shi, W. Synthesis of One-Molecule-Thick Single-Crystalline Nanosheets of Energetic Material for High-Sensitive Force Sensor. *Sci. Rep.* **2012**, *2*, 698.